Chapter IV
Intersubband terahertz absorption and photocurrent dynamics in quantum well infrared photodetector structures

4.1 Introduction

Since the initial proposal by Esaki and Tsu [1] and the advent of molecular beam epitaxy (MBE), interest in semiconductor superlattices (SLs) and quantum well (QW) structures has increased continuously over the years, driven by technological challenges and new physical concepts and phenomena as well as promising applications. A new class of materials and heterojunctions with unique electronic and optical properties has been developed. Here we focus on devices which involve infrared (IR) excitation of carriers in quantum wells. A distinguishing feature of QW infrared detectors is that they can be implemented in chemically stable wide-band-gap materials as a result of the use of intersubband processes. Among the different types of quantum well infrared photodetectors (QWIPs), the technology of GaAs/AlGaAs multiple-quantum-well (MQW) detectors is the most mature [2]. Rapid progress has been made recently in the performance of these detectors. Detectivities have improved dramatically and they are now high enough for the fabrication of large focal plane arrays with a long-wavelength IR imaging performance.

Many QWIPs which detect 10 μm-radiation have been fabricated, since wavelength nicely matches with a blackbody radiation at 300 K. In addition, in order to study the dependence of the optical and electrical properties on the number of quantum wells, QWIPs containing from 2 to 100 wells have also been investigated. The first QWIP was demonstrated by Levine et al. [3]. It consists of quantum wells containing two bound states. An infrared absorption due to intersubband transition from the bound ground state

to the bound excited state is followed by the tunneling of photoexcited electrons out of the well. These photocarriers, which escape QWs, are accelerated by the electric field into the continuum above the barriers for an excited-state life time during which they travel a distance of the mean free path for recapture back into the quantum well and, thereby, produce a photocurrent.

Although numerous experimental [2-8] and theoretical [9,10] studies have been conducted on multiple quantum well infrared photodetectors, single quantum well infrared photodetectors (SQWIPs) are particularly interesting since they have simple band structures, allowing accurate calculation of the bias voltage dependence of the potential profiles of each of two barriers, photo-induced band bending effects in the contacts, as well as charge accumulation in the quantum well [15-21]. By comparing theory with experiment, one can obtain a deeper understanding of the optical and transport properties in the QWIPs [15-21].

For this study we employed a conventional single quantum well structure which has emitter and collector contacts. Schematic conduction band diagram of a SQWIP is shown in Fig. 4.1 [17]. Under an applied bias voltage of V_b across the entire structure from the emitter to the collector contact, a current $I_e(V_e)$ will be injected via field emission from the emitter contact by the voltage drop V_e across the emitter barrier. In addition, a current $I_w(V_c)$ will also be generated from the quantum well composed of both a field-emission component $I_w^{fe}(V_c)$ and an optically excited component $I_w^{opt}(V_c)$ by the voltage drop V_c across the collector barrier. The applied voltage of the emitter barrier V_e is higher than that of the collector barrier V_c so that the current flowing from the emitter may meet the QW requirement. This band bending effect strikingly occurs when photoinduced carriers escape from the quantum well [18-21]. So far, attention has mainly been paid to the static characteristics of SQWIPs. However, an understanding of the dynamical characteristics is expected to yield more direct information on the physical process in the quantum well infrared photodetectors [22,23].

In this chapter, we have investigated the steady-state and dynamical aspects of

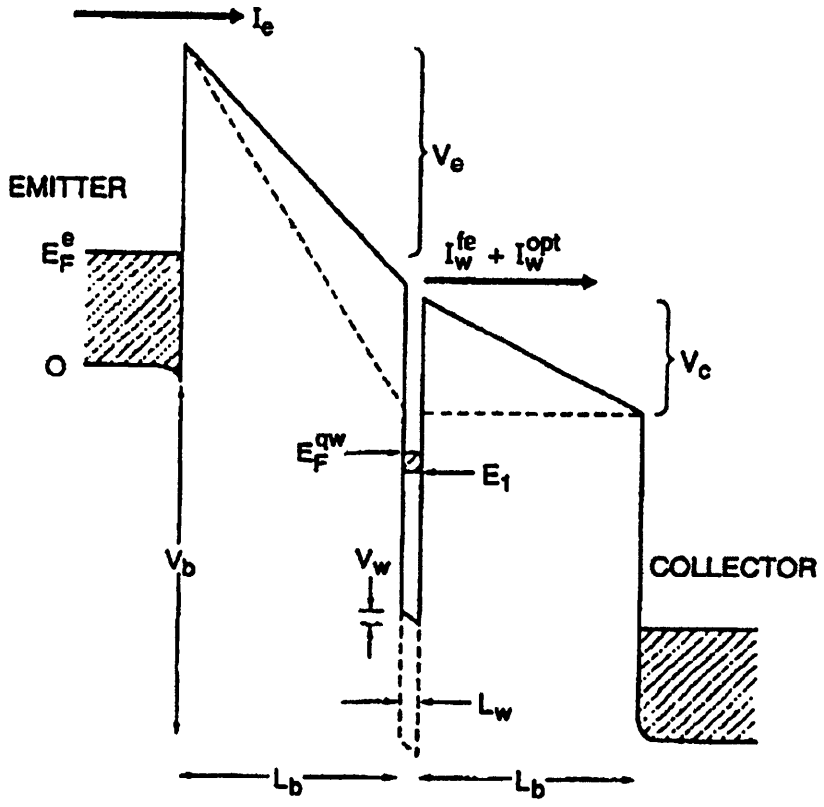

Fig. 4.1 Schematic conduction-band diagram of a single-quantum-well infrared photodetector. The solid line is in the dark; the dashed line is under illumination [2].

$Al_{0.3}Ga_{0.7}As$/GaAs SQWIPs. In the second section, the steady-state characteristics of the SQWIP is presented, which show a narrowband photocurrent at around 9.2 μm due to the intersubband transition in the steady state characteristics measured by using a Fourier transform infrared spectrometer. The bias voltage dependence of the magnitude and the spectral shape of the observed steady state photocurrent indicate that the photocurrent is strongly affected by the tunneling escape process. Furthermore, in the third section, the transient photoresponse of the SQWIP has been studied by free electron laser (FEL) pulses. A comparison of the steady state photocurrent and the transient photoresponse shows that the charging current induced by the band bending effect contributes to an increased photosensitivity. Numerical consideration of tunneling escape process in the SQWIP is presented in the forth section.

4.2 Steady state characteristics of single quantum well structures

4.2.1 Sample structure of single quantum well

Figure 4.2 shows a band diagram of the conduction band edge of the SQWIP, and a schematic illustration of the device structure studied in this work. The GaAs/$Al_{0.3}Ga_{0.7}As$ SQWIPs were grown on semi-insulating GaAs substrates by molecular beam epitaxy. The investigated *bound-to-bound* SQWIP structure consisted of an L_w = 60 Å GaAs quantum well (doped with Si, $N_D = 1\times10^{18}$ cm^{-3}) surrounded by two L_b = 500 Å undoped $Al_{0.3}Ga_{0.7}As$ barriers. This was designed to yield two bound states in the quantum well. The active region was sandwiched between similarly doped top (0.5 μm) and bottom (1 μm) ohmic contact layers. All of the SQWIPs were processed into 0.4 × 0.4 mm^2 mesas. AuGe/Ni/Au was evaporated on the top of the mesas and In was soldered for the bottom contacts. The substrate beneath the mesa was polished at 45° to allow optical coupling to the active region.

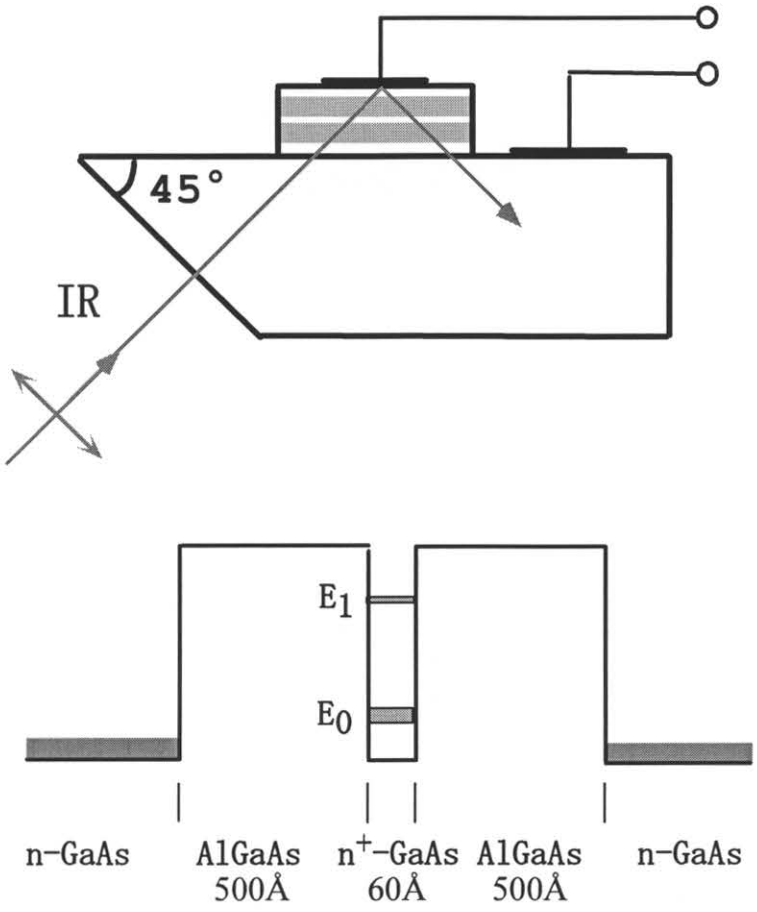

Fig. 4.2 (a) Device structure and (b) schematic illustration of band diagram of the multiple quantum well diode investigated in this study.

4.2.2 Current-voltage characteristics

Figure 4.3 shows a dc current-voltage (*I-V*) characteristic of the SQWIP, measured using a semiconductor parameter analyzer. The dark current measured at 4.2 K in a radiation tight cryostat is plotted by a solid line. The photocurrent measured at 10 K under a broadband illumination from a globar light source is shown by a dashed line and the photocurrent for an illumination with 1/20 intensity is shown by a dotted line. The photocurrent is the total current of the sample under illumination. It is found that there are two bias regions of the SQWIP photosensitivity; i.e., $0 < V_B < 0.2$ V and $0.2 \text{ V} < V_B < 0.5$ V. At $V_B \sim 0.2$ V, there is a clear kink in the photocurrent. This fact suggests that there are two components in the photocurrent when $V_B > 0.2$ V, the mechanism of which will be discussed later. The photocurrent for a reduced intensity exhibits a similar curve.

Figure 4.4 shows a temperature dependence of dark current for the SQWIP. In the Fig. 4.4 the dashed line is the photocurrent from the ambient background radiation through the Dewar window at $T = 10$ K. By comparing the temperature dependent dark current with the observed photocurrent, the background limited performance (BLIP) of the present device was obtained up to 65 K.

4.2.3 Photocurrent response

Figure 4.5 shows the steady state photocurrent spectra of the SQWIP measured for various V_B using a Fourier transform infrared spectrometer at $T = 10$ K. The photocurrent shows a narrowband peak at around 9.2 μm with a spectral width of $\Delta\lambda = 0.9$ μm. This observed narrowband spectrum indicates that the photocurrent is induced by an intersubband transition between the ground and the first excited subbands in the quantum well. As seen in the figure, the spectral shape of the photocurrent is slightly asymmetric; the photocurrent on the longer wavelength side (low energy side) of the peak decays more rapidly. This is due to the fact that although the intersubband photoexcitation spectrum of the electrons in the quantum well has a symmetric Lorentzian lineshape the tunneling

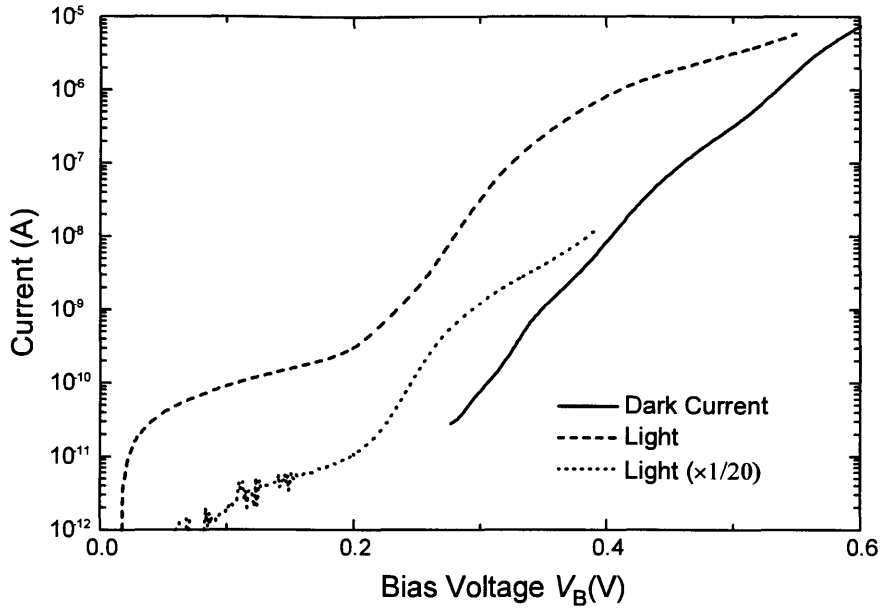

Fig. 4.3 The dark current measured at 4.2 K in a radiation-tight cryostat (solid line), the photocurrent measured at 10 K under illumination from a globar light source (dashed line) and the photocurrent for illumination with a power reduced by 1/20 (dotted line). The inset shows a schematic illustration of the band diagram.

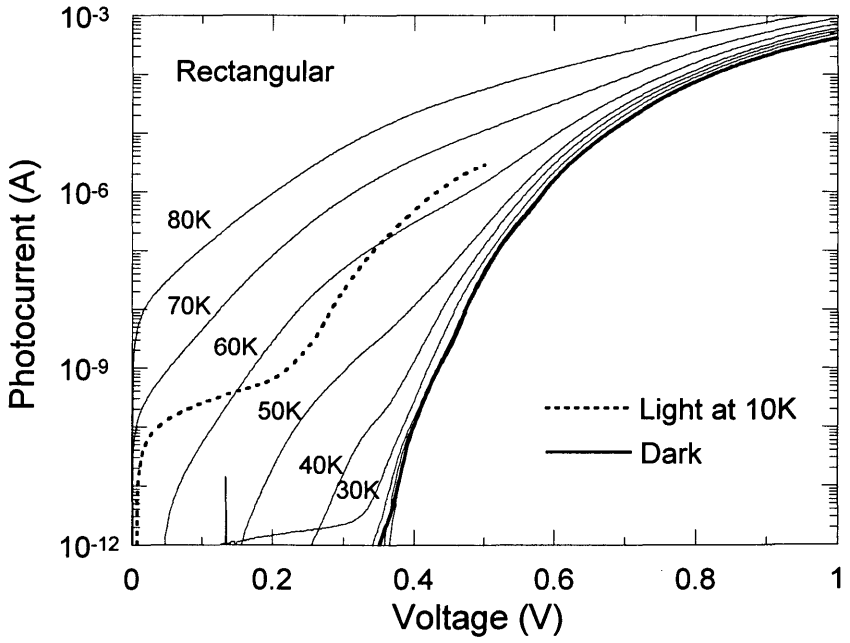

Fig. 4.4 Dark current bias curves (solid) as a function of temperature. The dashed line is the photocurrent from the ambient background radiation through the Dewar window. .

escape rate of the photoexcited electrons is lower for the low energy electrons and higher for the high energy electrons. Furthermore, it is found that the peak wavelength of the photocurrent gradually shifts to the shorter wavelength side as the bias voltage is decreased. This is because the cutoff wavelength of the tunneling escape process shifts to the shorter wavelength side as the bias voltage is decreased. Furthermore, the magnitude of the photocurrent decreases exponentially as the bias is reduced, indicating that the magnitude of the photocurrent is controlled by the tunneling escape process.

Figure 4.6 shows the bias-voltage dependence of the peak position and the magnitude of the photocurrent. It is found that the peak wavelength of the photocurrent gradually shifts to the shorter wavelength side as the bias voltage is decreased. This is because the cutoff wavelength of the tunneling escape process shifts to the shorter wavelength side as the bias voltage is decreased. Furthermore, the magnitude of the photocurrent decreases exponentially as the bias is reduced, indicating that the magnitude of the photocurrent is controlled by the tunneling escape process.

4.3 Photocurrent dynamics of single quantum well structures

4.3.1 Introduction

Although attention has been paid mainly to the static characteristics of SQWIPs, an understanding of dynamical characteristics is expected to yield more direct information on the physical process in the quantum well infrared photodetectors. In this section, the transient photoresponse of the rectangular SQWIP is investigated by using free electron laser (FEL) pulses. A comparison of the steady state photocurrent and the transient photoresponse shows that the charging current induced by the band bending effect contributes to an increased photosensitivity.

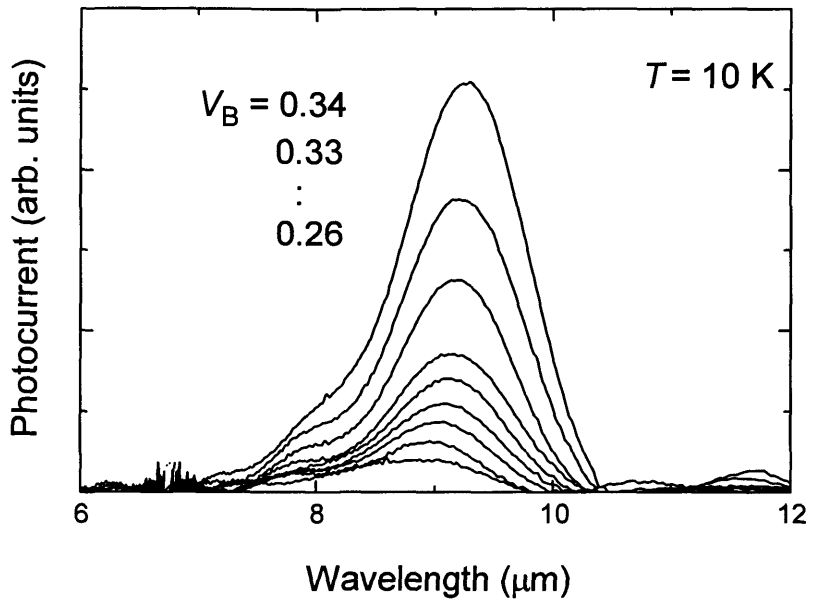

Fig. 4.5 The photocurrent spectra measured at 10 K for various applied voltages from 0.26 to 0.34 V with a voltage step of 0.01 V.

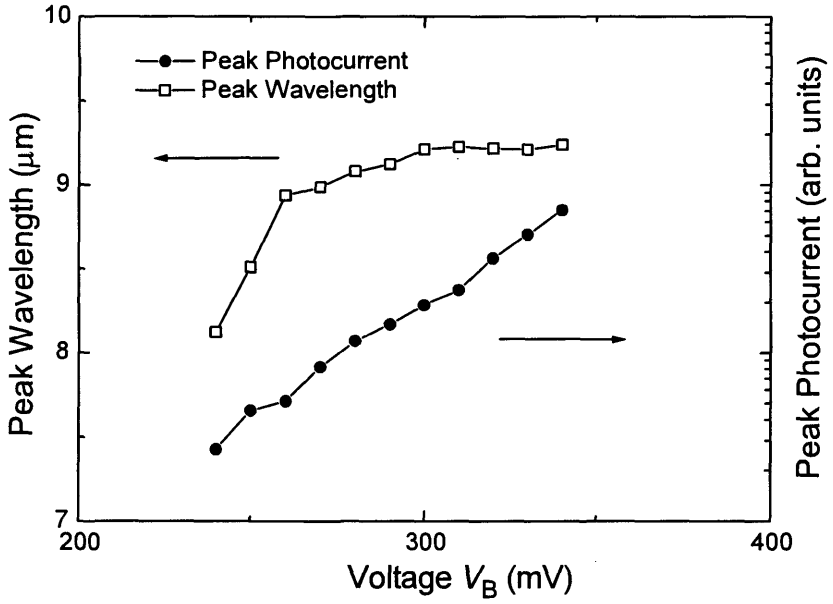

Fig. 4.6 The bias-voltage dependence of the peak position and the magnitude of the photocurrent.

4.3.2 Experimental setup using free electron laser

In order to establish a clearer knowledge on the tunneling escape process and the band bending effect, we have investigated the photocurrent dynamics of the SQWIP by using FEL pulses. A linac-driven FEL system has been developed at Free Electron Laser Research Institute, covering a wide range of spectra from ultraviolet to far-infrared (Fig. 4.7) [24]. The FEL has several attractive features, including its ultra-short pulse width and high peak power and the wide tunability of the lasing wavelength. The FEL delivers macropulses with widths of 15 μs at 10 Hz repetition rate. Each macropulse has a train of about 300 ultra short micropulses with a 45 ns separation. The width of the optical micropulse is estimated to be about 3 ps (Fig. 4.7). The peak power of a micropulse is of the order of 1 MW. Even though the peak power is very high, the average power is low (~10 mW) due to a low duty ratio. The FEL wavelength is tuned to be 9.2 μm, in order to resonantly excite the intersubband transition in the SQWIP (Fig. 4.8). Figure 4.9 shows the experimental setup for the FEL measurements. The FEL beam is focused on the polished 45° face of the SQWIP with a ZnSe lens. The sample is mounted in a cryostat and kept at 10 K. We analyzed the transient response of the photocurrent synchronized to the FEL macropulses. The signal was monitored with a digitizing oscilloscope through a current amplifier.

4.3.3 Transient photocurrent response

Figure 4.10 shows the photocurrent transients measured for V_B. As seen in the figure, the observed photocurrent response almost instantaneously follows the waveform of the FEL macropulses when $V_B \leq 0.3$ V. However, when $V_B \geq 0.4$ V, the transient photoresponse, with a large initial spike and slow decay components, was observed. The potential profile in the single quantum well structure is determined by the charging state in the quantum well and is controlled by the balance between the emitter current and the photo-induced current. Since the intensity of one micropulse is 1 MW, most of the

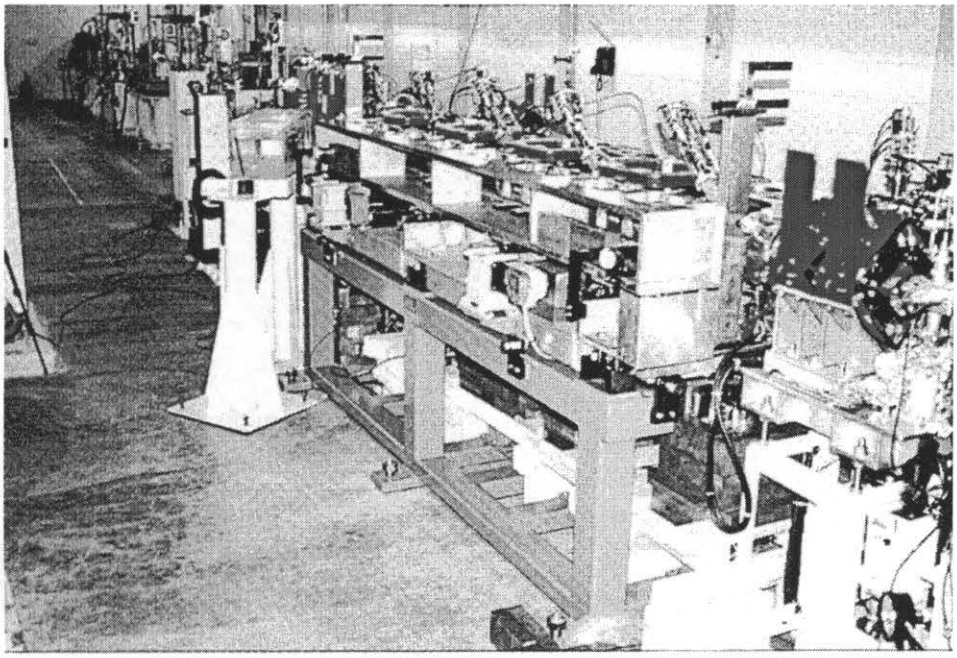

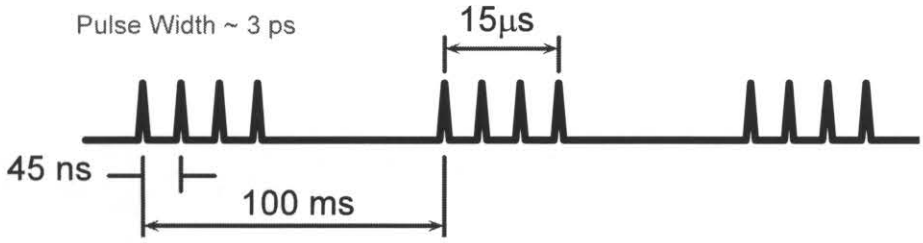

Fig. 4.7 Upper panel shows a free electron laser facility in FEL Institute. Lower panel shows a time chart of emitted laser pulse train induced by the FEL.

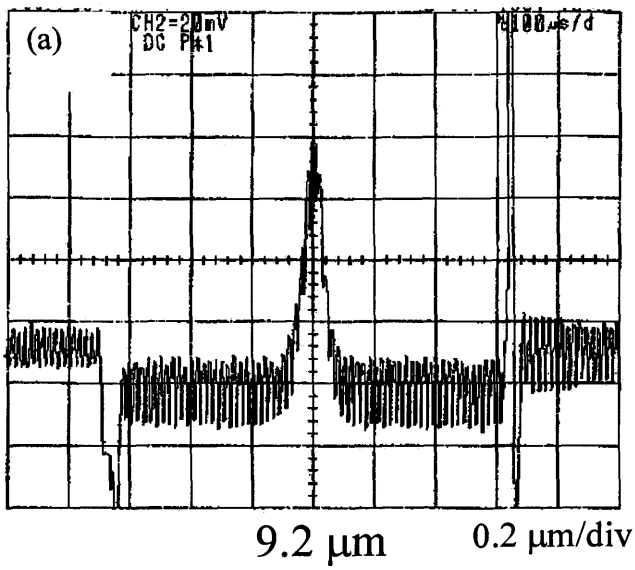

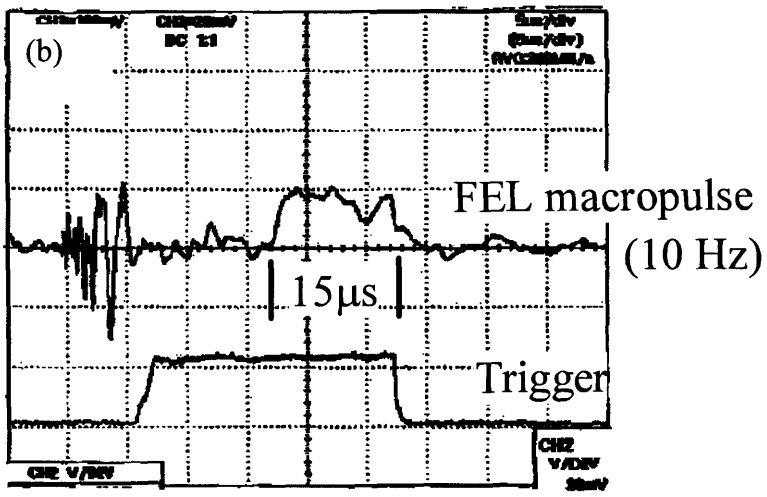

Fig. 4.8 (a) Spectrum of the FEL pulse tuned to λ = 9.2 μm. (b) Pulse width of the FEL macro pulse.

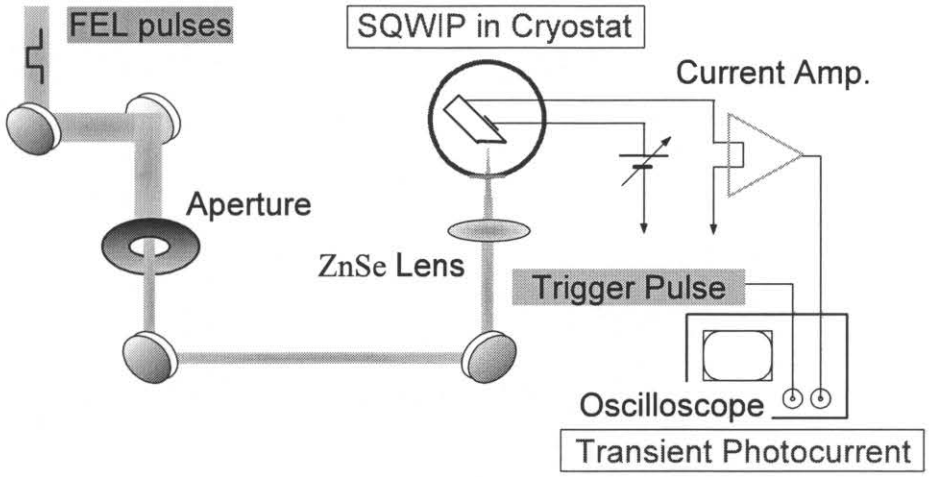

Fig. 4.9 Schematic illustration of a setup for transient response measurement of SQWIP by using free electron laser pulses.

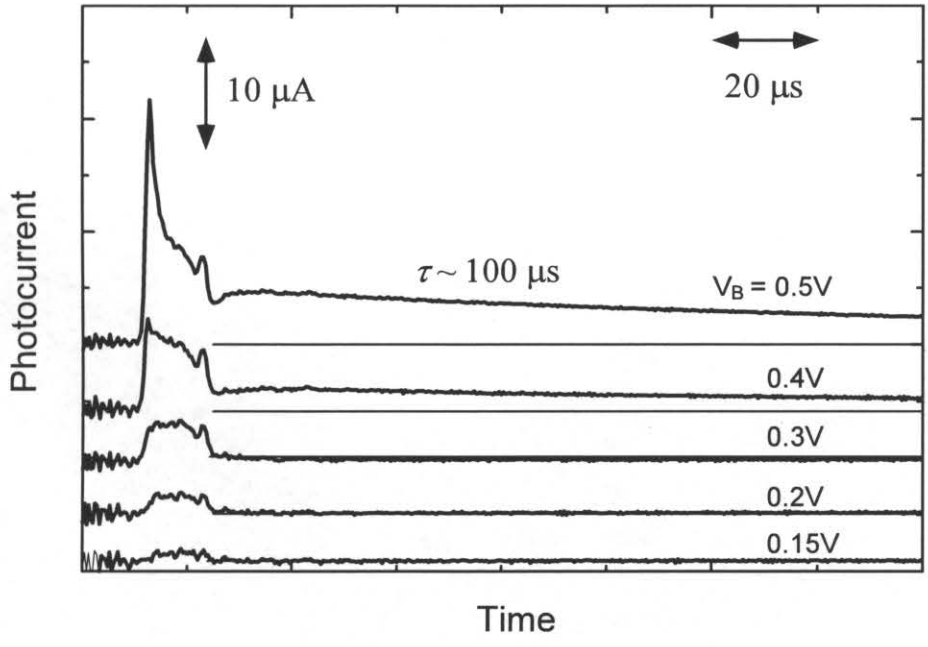

Fig. 4.10 The photocurrent transients for various applied bias voltages to the FEL macropulses.

electrons in the quantum well are excited from the ground to the first excited state when the first shot of the FEL micropulses hits the SQWIP. When the bias voltage is low, however, only a small portion of the photoexcited electrons are emitted to the collector because of the small tunneling escape rate. In such a case, the emitter current is large enough to compensate for the reduction of electrons and the quantum well can be kept almost neutral. Therefore, the photocurrent follows the waveform of the input FEL macropulses (direct process). On the other hand, when the bias voltage is high, a larger portion of the photoexcited electrons can escape from the quantum well. This depletion of the electrons leads to positive space charges in the quantum well. In order to compensate for this positive space charge, an extra current injection from the emitter is required. Therefore, even after the FEL macropulse is turned off, the quantum well is charged from the emitter through the tunneling resistance. This process has a long time constant of the order of 100 μs (charging process).

4.3.4 Bias voltage dependence of charging process

Figure 4.11 suggests that the steady state photocurrent consists of only one component in the low bias region ($V_B \leq 0.2$ V) and that there are two components in the high bias region ($0.2 \leq V_B \leq 0.5$ V). In the transient photocurrent measurements, only a fast direct photoexcitation component was observed in the low bias region, while two components, *i.e.* the fast component and the slow charging component, were observed in the high bias region. A comparison of the steady state and the transient photoresponse concludes that the slow charging process contributes to a large photosensitivity observed for $V_B > 0.2$ V.

From the discussion above, it is expected that the onset of the slow charging process depends not only on V_B but also on the intensity of the incident radiation. However, even when the incident light power was reduced by 1/20, the onset of the charging component did not shift significantly, as shown by a dotted line in Fig. 4.3. Furthermore, Fig. 4.12

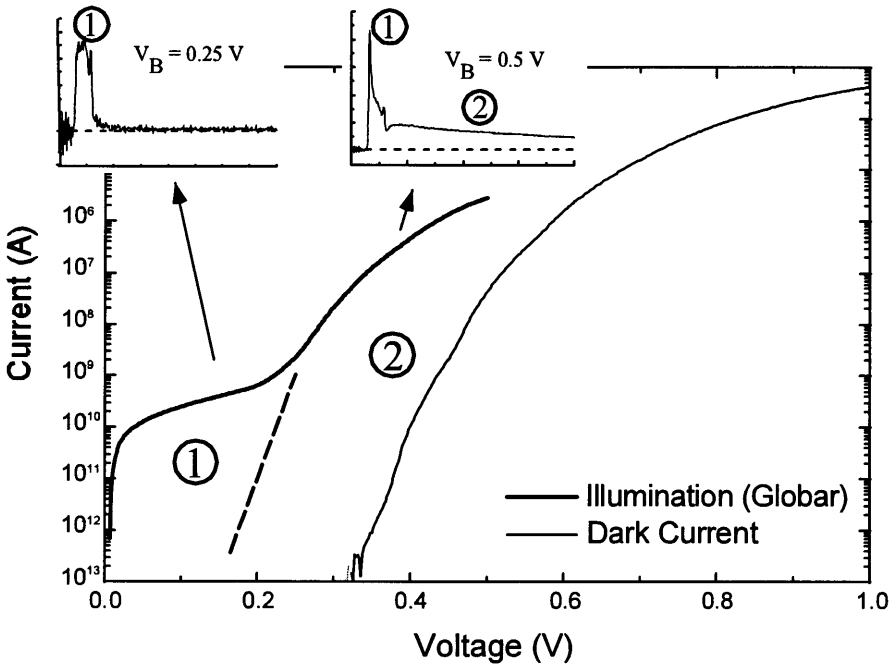

Fig. 4.11 Current-voltage characteristics under illumination and dark condition as shown in Fig 4.3. Two distinct regions are recognized in photocurrent. Insets show the transient photocurrent response for each bias region.

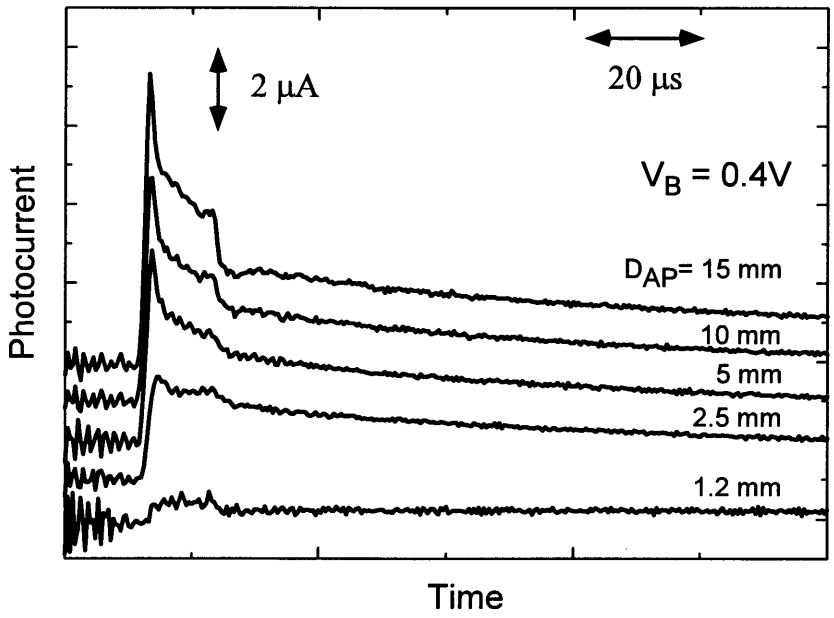

Fig. 4.12 Dependence of the photocurrent transients on the FEL intensity measured at V_B = 0.4 V. The FEL intensity was controlled by using a mechanical aperture. The aperture diameters D_{AP} were varied from 1.2 to 15 mm.

shows the FEL power dependence of the photocurrent measured for various aperture diameters D_{AP} at V_B = 0.4 V. As seen in the figure, the slow charging currents with almost identical magnitudes were observed for all the D_{AP}'s studied here, except for the case of a very weak excitation (D_{AP} = 1.2 mm). This fact indicates that the onset of the charging process is controlled predominantly by the strong V_B dependence of the tunneling escape process and not by the intersubband excitation process.

4.4 Numerical consideration of single quantum well infrared photodetector

4.4.1 Introduction

Although numerous experimental and theoretical studies have been conducted on multiple quantum well infrared photodetectors, single quantum well infrared photodetectors (SQWIPs) are particularly interesting since they have simple band structures, allowing accurate calculation of the bias voltage dependence of the potential profiles of each of the two barriers, photo-induced band bending effects in the contacts, as well as charge accumulation in the quantum well. In this section, we show a theoretical analysis of a band bending effect due to tunneling escape process in the SQWIP.

4.4.2 Theoretical model of tunneling current under dark condition

Figure 4.13 shows a schematic conduction band diagram of a SQWIP considered here at an applied bias voltage of V. Two quantized states are formed in the quantum well. Under an applied bias voltage of V across the entire structure from emitter to the collector contact, a current $J_e(V_e)$ will be injected via field emission from the emitter contact by the voltage drop V_e across the emitter barrier. In addition, a current $J_w(V_c)$ will also be generated from the quantum well composed of both a field emission component $J_{qw}^0(V_c)$ and an optically excited component $J_{qw}^1(V_c)$ by the voltage drop V_c across the collector

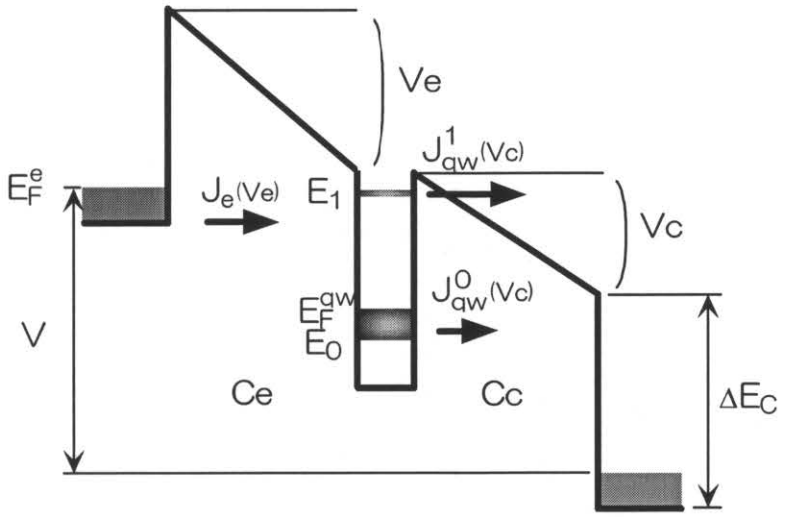

Fig. 4.13 Schematic illustration of band diagram for theoretical analysis of tunneling current with an applied bias voltage *V*.

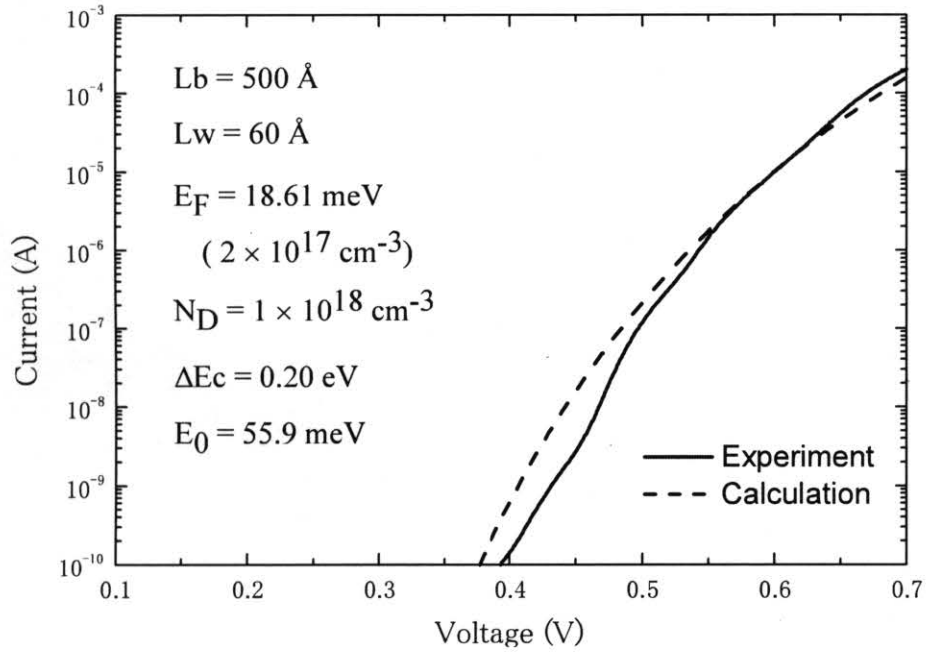

Fig. 4.14 Current-voltage characteristics for dark condition. Dashed and solid lines are a calculated and experimental dark current, respectively. Parameters used for the calculation are also listed in the figure

barrier. These current and voltage are related as

$$eL_w(N_D - n) = C_e V_e - C_c V_c \tag{4.1}$$

$$J_e(V_e) = J_{qw}^0(V_c, n) \tag{4.2}$$

for the dark condition, and

$$J_e(V_e) = J_{qw}^0(V_c, n) + J_{qw}^1(V_c, n) \tag{4.3}$$

for the light condition, where $V = V_e + V_c$, n is the three-dimensional free-carrier density in the well, C_e and C_c are the capacitance of the emitter and collector, respectively. The expression for the three-dimensional emitter current J_e and two-dimensional quantum well field emission current J_{qw} are given

$$J_e(V_e) = \frac{emkTA}{2\pi^2\hbar^3}\int_0^\infty T_{(E,V_e)} \ln\left(1 + \exp\left(\frac{E_{F_e} - E}{kT}\right)\right) dE \tag{4.4}$$

and

$$J_{qw}(V_c) = \frac{em}{2\pi\hbar^2 L}\upsilon \int_{E_c}^\infty T_{(E,V_c)} \frac{1}{1 + \exp\left(\frac{E - E_0 - E_{F_{qw}}}{kT}\right)} dE \tag{4.5}$$

where $L = (L_w + L_b)$, and E_{Fe} and E_{Fqw} are Fermi energies in the emitter (with respect to the bottom of the conduction band) and the quantum well (with respect to the ground-state energy), respectively. The energy-dependent transmission coefficients of the emitter and collector barriers are $T(E,V)$. Equations (4.4) and (4.5) describe currents flowing from the emitter to the collector; although there are current components flowing in the reverse direction, they are negligible for all the bias conditions studied here. Using Eqs. (4.1)-(4.5), the theoretical dark currents can be calculated, and are compared with experiment for T = 10 K in Fig. 4.14. The excellent agreement in the dark current is obtain by using the parameters listed in Fig. 4.14.

4.4.3 Theoretical model of photo-induced tunneling current

Next, let us discuss a theoretical analysis of the band bending effect due to

photoresponse in the SQWIP. Figure 4.15 shows schematic illustration of band diagram of the single quantum well structure for theoretical analysis of photo-induced tunneling current. When an infrared power P is absorbed in the quantum well, rate equations which describe the carrier densities for the quantized states in the well are given as

$$\frac{dN_0}{dt} = -\frac{P}{h\nu} + \frac{N_1}{\tau_L} - \frac{N_0}{\tau_0}, \tag{4.6}$$

$$\frac{dN_1}{dt} = \frac{P}{h\nu} - \frac{N_1}{\tau_L} - \frac{N_1}{\tau_1}, \text{ and} \tag{4.7}$$

$$n = N_0 + N_1, \tag{4.8}$$

where N_0 is the carrier density for the ground state, N_1 the carrier density for the excited state, τ_L the intersubband relaxation time in the quantum well (0.8 ps), and τ_1 the tunneling escape time for the electrons on the excited state (Fig. 4.15).

Under a steady state condition, $dN_1/dt = 0$. From (4.6) – (4.8), the photoinduced current I_p is given as

$$N_1 = -\frac{P}{h\nu} \cdot \tau_L \cdot \left(1 + \frac{\tau_L}{\tau_t}\right)^{-1} \tag{4.9}$$

$$I_p = e \cdot N_1 \cdot \tau_t^{-1} \tag{4.10}.$$

The obtained formula can be used for evaluation of the performance of SQWIPs under an illumination. Fig 4.16 shows a comparison between the calculated and measured current-voltage characteristics for the dark and light conditions. The bold dashed line denotes the measured dark current, and the bold solid line shows the measured photocurrent under an illumination from a globar. Thin dashed lines denote the calculated photocurrents for various infrared powers. The measured voltage dependence of the photocurrent is in good agreement with the theory. By comparing with the experiments and calculations, the absorbed light power is estimated to be about 100 pW.

The responsivity R of QWIP is given in term of the photocurrent I_P and the incident light power P as $R = I_P/P$. According to the above calculation, an essential responsivity of the SQWIP is estimated to be $R \sim 100$ A/W, which is larger than conventional QWIP.

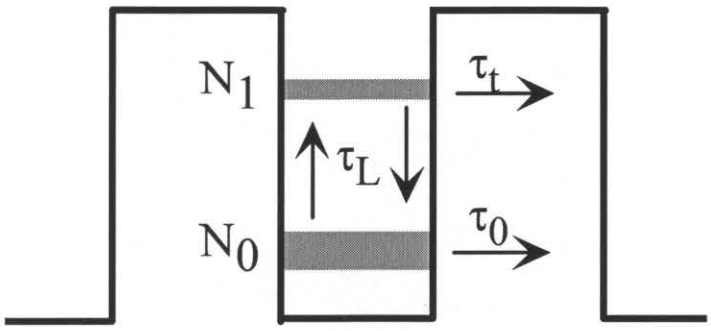

Fig. 4.15 Schematic illustration of band diagram of the single quantum well structure for the theoretical analysis of photo-induced tunneling current. τ_L is the intersubband relaxation time. τ_0 and τ_1 are the tunneling escape times for electrons in the ground and the first excited levels, respectively. N_0 and N_1 are the carrier densities for each quantized level.

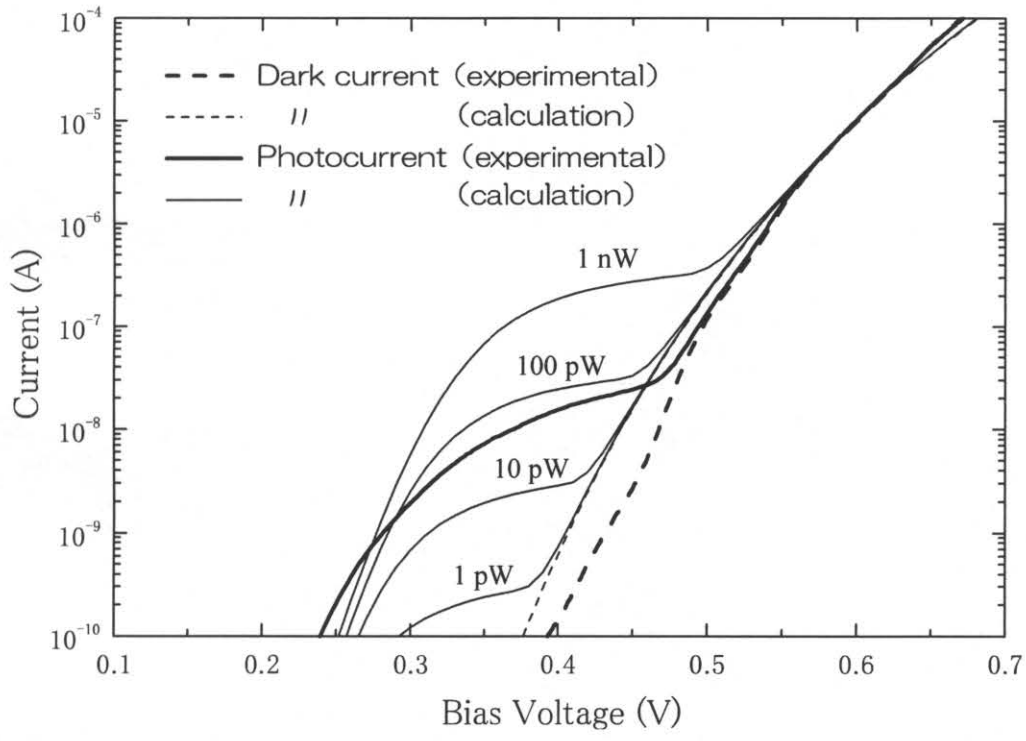

Fig. 4.16 Comparison between experimental and calculated current-voltage characteristics under dark and light condition.

Therefore, SQWIP is expected to be high performance infrared photodetectors.

4.4.4 Large photoconductivity due to band bending effect

Next, let us consider the band bending effect in the quantum well. Calculated voltage drops V_c and V_e under a current continuity condition are plotted in Fig. 4.17. The solid line shows a dark condition. The dotted and dashed lines show light conditions for an incident power $P = 100$ and 10 pW, respectively. It is noted that the voltage drop at the emitter barrier V_e is always larger than that at the collector barrier V_c. The reason for this small collector bias is the large tunneling probability through the collector barriers. Note that the collector potential V_c increases approximately linearly with applied bias voltage at dark condition. For the light condition, the collector potential drop V_c becomes negative for $V_B < 0.2$ and the band structure is shown as Fig. 4.17(b). Furthermore, extreme band bending effects are expected in the light condition to satisfy the current continuity between the emitter current and photoinduced current. This behavior is a result of a dramatic decrease in carrier density n in the quantum well under illumination. This drop in n produces a corresponding decrease in V_c (and increase in V_e)

As shown in Fig. 4.10, a large charging current is observed in the transient response of photocurrent at $V_B > 0.3$ V. The charging process indicates that the SQWIP has highly sensitivity due to the long life time of photo-induced carriers. In order to further understanding this unique behavior of the transient response we have considered the band bending effect under FEL irradiation. Figure 4.18 shows the calculated band profiles and the related energy dispersions of the SQWIP at $V_B < 0.2$ V (Fig. 4.18(a)), and $V_B > 0.3$ V (Fig. 4.18(b)). The bold and dashed lines show the band profiles under and after FEL irradiation, respectively. When the FEL pulse is irradiated to the SQWIP, the photo-induced carriers escape from the quantum well and the carrier density in the quantum well decreases. After the FEL pulse is turned off, the quantum well is recharged through both of emitter and collector barriers. At $V_B < 0.2$ V, the ground state of the

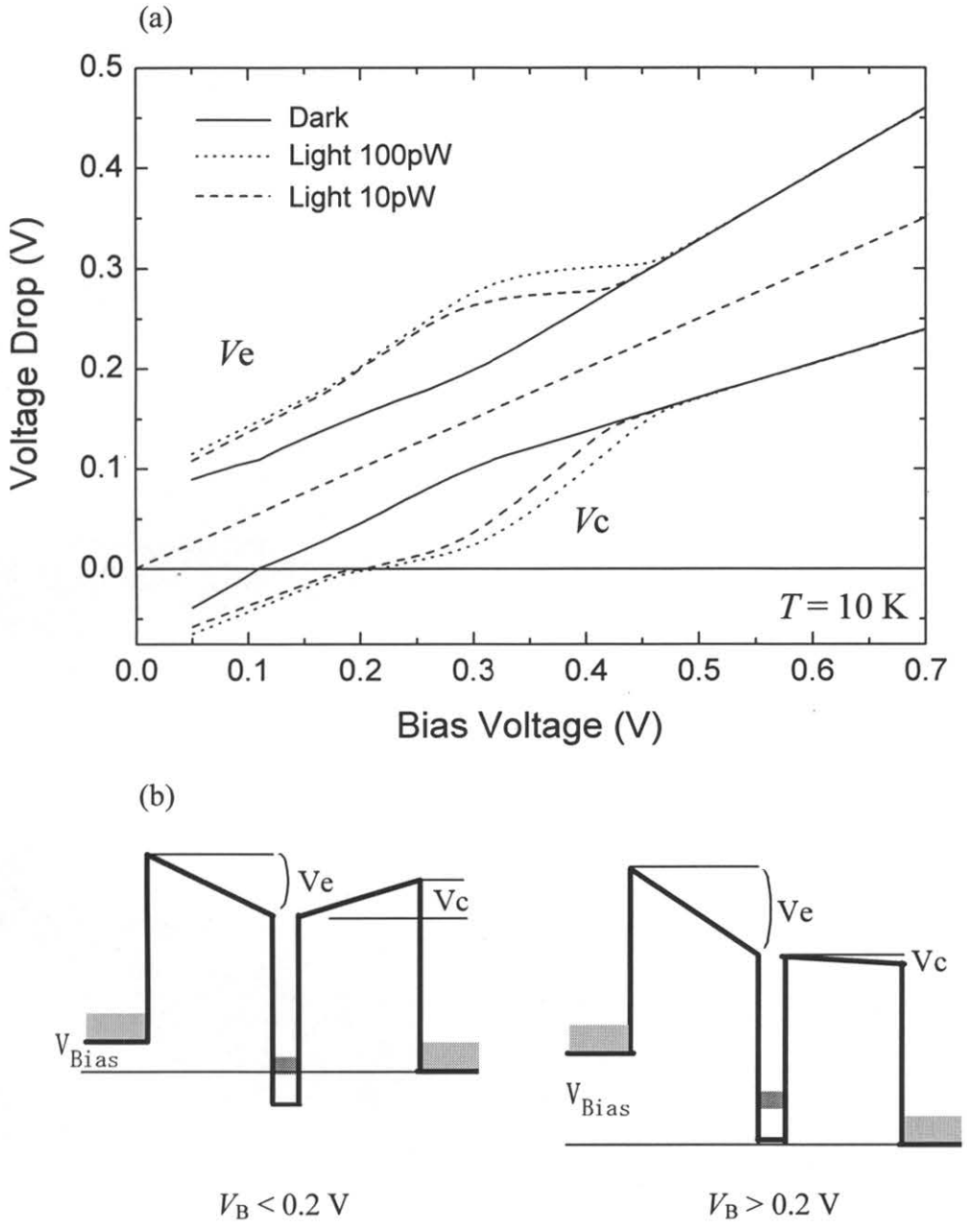

Fig. 4.17 (a) Voltage drop of emitter (V_e) and collector (V_c) barriers and applied total voltage and (b) schematic illustration of band bending for $V_B < 0.2$ V and $V_B > 0.2$ V.

quantum well is almost consisted with the Fermi level of collector at all times. The recharge time becomes fast due to the large resonant current through the collector. The sensitivity of the SQWIP is not high in this bias region because of the short life time of photocarriers. At $V_B > 0.3$ V, the ground state of the quantum well is rather separated from the Fermi level of collector. After the FEL pulse is turned off, the recharging process is caused by only the emitter current which is not large enough to charge the quantum well, and the charging time becomes long. Therefore the SQWIP has highly sensitivity due to the very long life time of photo-induced carriers at higher bias region. The life time of carriers becomes remarkably large as the bias voltage increases because of the large electron depletion in the quantum well. Thus, the optical and transport properties of a rectangular barrier SQWIP is understood in terms of the potential drops across the individual barriers, the photoinduced electron depletion in the quantum well, and unusual bias dependence of the photocurrent.

4.5 Summary of Chapter IV

In this chapter, we have studied the optical and transport properties of SQWIPs. Using the Fourier transform infrared spectrometer, we measured the steady state characteristics of the photocurrent, which showed a narrowband photocurrent at around 9.2 μm due to inter-subband transition. The bias voltage dependence of the magnitude and the spectral shape of the observed photocurrent indicated that the photocurrent was strongly affected by the tunneling escape process. Furthermore, we have investigated the photocurrent dynamics by free electron laser pulses. A comparison of the steady state photocurrent and the transient photo-response showed that the charging current induced by the band bending effect contributes to an increased photosensitivity. Numerical consideration of the SQWIP strongly supported the band bending effect due to photo-induced carriers.

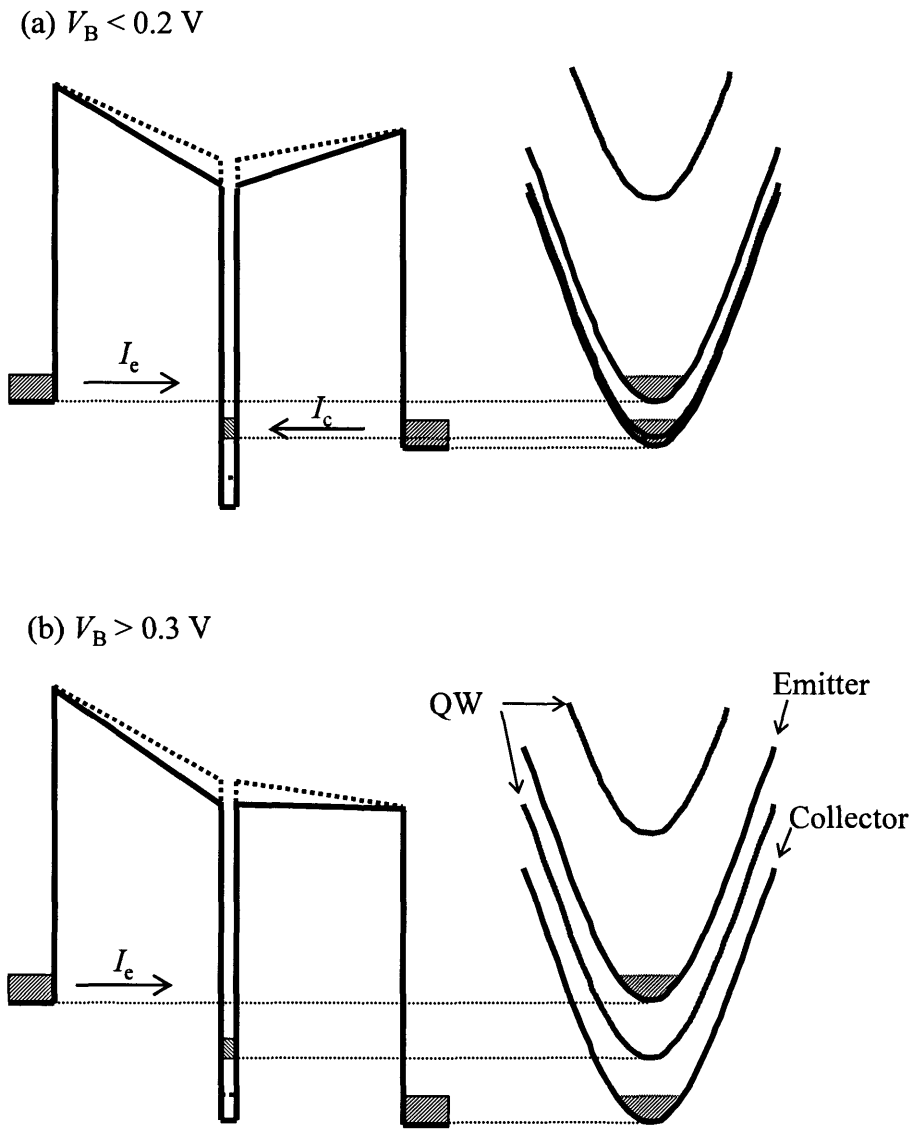

Fig. 4.18 (a) Calculated band profile and the energy dispersion of the SQWIP at $V_B < 0.2$ V, (b) and $V_B > 0.3$ V. The bold and dashed lines show the band profiles under and after FEL irradiation, respectively.

Bibliography

[1] L. Esaki and R. Tsu, IBM J. Res. Dev. **14**, 61 (1970).

[2] B. F. Levine, J. Appl. Phys. **74**, R1 (1993).

[3] B. F. Levine, C. G. Bethea, G. Hasnain, J. Walker, and R. J. Malik, Appl. Phys. Lett. **53**, 296 (1988).

[4] K. K. Choi, B. F. Levine, C. G. Bethea, J. Walker, and R. J. Malik, Appl. Phys. Lett. **50**, 1814 (1987).

[5] B. F. Levine, C. G. Brthea, G. Hasnain, V. O. Shen, E. Pelve, R. R. Abbott, and S. J. Hsieh, Appl. Phys. Lett. **56**, 851 (1990).

[6] B. F. Levine, A. Zussman, S. D. Gunapala, M. T. Asom, J. M. Kuo, and W. S. Hobson, J. Appl. Phys. **72**, 4429 (1992).

[7] Larry S. Yu, Y. H. Wang, Sheng S. Li, and Pin Ho, Appl. phys. Lett. **60**, 992(1994).

[8] S. D. Gunapala, K. M. S. V. Bandara, B. F. Levine, G. Sarasi, J. S. Park, T. L. Lin, W. T. Pike, and J. K. Liu, Appl. Phys. Lett. **64**, 3431 (1994).

[9] E. Pelve, F. Beltram, C. G. Bethea, B. F. Levine, V. O. Shen, S. J. Hsieh, and R. R. Abbott, J. Appl. Phys. **66**, 5656 (1989).

[10] S. R. Andrews and B. A. Miller, J. Appl. Phys. **70**, 993 (1991).

[11] Y. Zhang, D. S. Jiang, J. B. Xia, L. Q. Cui, C. Y. Song, Z. Q. Zhou, W. K. Ge, Appl. Phys. Lett. **68**, 2114 (1996).

[12] J. C. Chiang, S. S. Li, M. Z. Tidow, P. Ho, M. Tsai, and C. P. Lee, Appl. Phys. Lett. **69**, 2412 (1996).

[13] C. J. Chen, K. K. Choi, M. Tidrow, and D. C. Tsui, Appl. Phys. Lett. **68**, 1446 (1996).

[14] T. R. Schimert, S. L. Barnes, A. J. Brouns, F. C. Case, P. Mitra, and L. T. Claiborne, Appl. Phys. Lett. **68**, 2836 (1996).

[15] A. Zussman, B. F. Levine, J. M. Kuo and J. de Jong, J. Appl. Phys. **70**, 5101 (1991).

[16] H. C. Liu, G. C. Aers, M. Buchanan, Z. R. Wasilewski and D. Landheer: J. Appl. Phys. **70**, 935 (1991).

[17] E. Rosencher, F. Luc, Ph. Bois and S. Delaitre, Appl. Phys. Lett. **61**, 468 (1992).

[18] K. M. S. V. Bandara, B. F. Levine, and M. T. Asom, J. Appl. Phys. **74**, 346 (1993).

[19] K. M. S. V. Bandara, B. F. Levine, R. E. Leibenguth and M. T. Asom, J. Appl. Phys. **74**, 1826 (1993).

[20] A. Carbone and P. Mazzetti: Appl. Phys. Lett. **70**, 28 (1997).

[21] V. Ryzii and M. Ershov, J. Appl. Phys. **78**, 1214 (1995).

[22] S. Ehret, H. Schneider, C. Schönbein, G. Bihlmann and J. Fleissner: Appl. Phys. Lett. **69** (1996) 931.

[23] M. Ershov, Appl. Phys. Lett. **69**, 3480 (1996).

[24] T. Tomimasu, Y. Morii, E. Oshita, S. Abe, S. Nishihara, A. Koga, Y. Miyauchi, A. Zakou, E. Nishimura, K. Saeki, A. Kobayashi, M. Yasumoto, E. Tongu, and A. Nagai, Nucl. Instr. and Meth. A **358**, 11 (1995).

Chapter V

Conclusion

For device applications of the superlattices, it is essential to establish a good understanding of the mechanism of transport and optical dynamics. In addition to this, the field-induced tunneling dynamics of carriers also needs to be evaluated accurately for the structures. In this thesis, we have studied 'carrier dynamics of tunneling properties' of superlattices, and to show how terahertz (THz) emission spectroscopy can reveal some of the unique properties of the miniband structure and their aspects of the coherent electron motion in such structures.

In order to make clear tunneling phenomena and a formation of quantized states in weakly coupled superlattices (multiple quantum wells), we have fabricated GaAs/$Al_{0.3}Ga_{0.7}As$ semiconductor multiple quantum well structures and investigated electron transport properties. Periodic negative differential resistances due to sequential resonant tunneling and a formation of high field domains have been studied in detail. Furthermore, a sequential resonant magneto-tunneling through Landau levels have been shown by a characterization of tunneling current under high magnetic fields. Dynamics of a high field domain formation have been also discussed by analyzing temporal transport properties in multiple quantum wells using step and sweep bias fields. In the section 2.3, we have investigated the tunneling *I-V* characteristics of $Al_{0.3}Ga_{0.7}As$/GaAs MQW diodes with various electron densities, N_s, and scattering rates, Γ. Clear periodic NDRs are observed for the samples with low N_s and Γ, while no NDRs are observed in the *first* plateau region of the *I-V* characteristics of the samples with high N_S and Γ. We have shown that such formation/destruction of the high-field domains in MQW diodes is controlled by the interplay of the tunneling rate and the electron supply-functions between the adjacent coupled QWs. The technological

implication of the present result is that by carefully designing the structure and the doping level of MQW diodes it is possible to apply uniform electric field throughout the MQW structure, which would be suitable for realizing novel THz emission/detection devices. In the section 2.4, we have investigated the tunneling *I-V* characteristics of modulation-doped GaAs/$Al_{0.3}Ga_{0.7}As$ MQW structures under high magnetic fields *B*. It is found that the first plateau of the tunneling *I-V* characteristics of the MD-MQWs exhibits a couple of remarkable features; in particular, a strong dependence on a magnetic field, *B*, applied normal to the layer plane is observed. The observed NDRs are identified to be due to the scattering-assisted sequential resonant tunneling through successive Landau levels. Furthermore, the observed voltage spacings of NDRs are systematically smaller than the cyclotron energy. We have extended the theory developed by Kazarinov and Suris to a finite magnetic field case and found that all the observed features are well explained by the interplay between the scattering-assisted inter Landau-level tunneling and the *B* dependence of the two-dimensional electron supply function. We have also shown that the present tunneling spectroscopy allows us a unique opportunity to determine the Landau level width, Γ. The determined Γ is found to be strongly dependent on the Landau level filling factor through the screening effect. In the section 2.5, we have investigated the frequency and temporal dependence of the tunneling *I-V* characteristics of GaAs/$Al_{0.3}Ga_{0.7}As$ MQW sequential resonant tunneling diodes. The *I-V* characteristics show remarkable frequency dependences; i.e., the formation of high-field domains is not able to follow the high frequency applied electric fields. Furthermore, the temporal response of the tunneling current to a stepped voltage clearly exhibits a finite transient from the peak to valley current. It is found that such a finite time constant necessary to form high-field domains is well explained by the product of the capacitance of a tunneling barrier and the intrinsic tunneling resistance in the low-field domain.

It was of prime importance to understand a dynamical electron motion in the THz regime in order to realize ultra-fast devices based on superlattices. For this purpose, a

time-resolved THz emission spectroscopy has been established to investigate a dynamical electron motion in superlattices. We have fabricated m-i-n GaAs/$Al_{0.3}Ga_{0.7}As$ superlattice structures suited for THz emission measurements. Photo absorption properties have been investigated by photocurrent spectra using a Fourier transform spectroscopy, verifying a formation of minibands and Wannier-Stark ladders. THz emissions from the superlattices have shown a dynamical electron transport in minibands, involving the Bloch oscillations. The THz emission due to Bloch oscillations have been also observed at room temperature. Furthermore, we have shown a strong experimental support for the THz gain due to Bloch oscillating electrons in wide miniband GaAs/$Al_{0.3}Ga_{0.7}As$ SLs. Quasi-periodic structures have been observed in the emitted THz intensity-vs-bias field curve and identified to be due to the resonant Zener tunneling between the Wannier-Stark ladders associated with the ground and the excited minibands. In the section 3.4, we have investigated a direct observation of THz emission due to BO in wide miniband GaAs/AlGaAs superlattice m-i-n diodes by time-resolved THz spectroscopy. Quasi-autocorrelation measurements were performed on the emitted THz electromagnetic wave by using a bolometer as a wideband detector. We have found that the THz radiation is strongly dependent on the miniband width. Furthermore we have found that the THz emission due to miniband transport is strongly dependent on the photon energy of the pump laser pulses. The bias-field dependence of the emitted THz radiation intensity clearly showed a crossover from the miniband transport to the formation of WSL. In the WS regime, a few cycle BO were observed even at 300 K in a superlattice whose miniband width is greater than the LO phonon energy. In the section 3.5, we have investigated terahertz (THz) emission due to dynamical electron transport in wide miniband GaAs/$Al_{0.3}Ga_{0.7}As$ superlattices by time-domain THz emission spectroscopy. By noting that the time-domain THz spectroscopy inherently measures the step-response of the electron system to the bias electric field, the obtained THz spectra were compared with theoretically predicted high-frequency conductivity. Excellent agreement between theory and experiment strongly supports that the THz gain due to Bloch oscillating electrons in

wide-miniband superlattices persists at least up to 1.7 THz. In the section 3.6, we have investigated the THz emission induced by high-field electron transport in biased wide-miniband GaAs/$Al_{0.3}Ga_{0.7}As$ superlattices. With increasing bias fields, two distinct regimes are observed in the bias-field dependence of the emitted THz intensity. These two regimes are attributed to the intra-miniband transport and inter-miniband Zener tunneling regimes, respectively. In the inter-miniband Zener tunneling regime, quasi-periodic structures are observed in the bias field dependence of the emitted THz intensity. It is found that the quasi-periodic peak structure was identified to be due to the resonant Zener tunneling between the Wannier-Stark ladders associated with the ground and excited minibands. Resonant Zener tunneling into the first and second excited state was clearly resolved.

Single quantum well infrared photodetectors were particularly interesting since they had exceptionally high optical gain and, in addition, their simple band structures allowed accurate calculation of the bias voltage dependence of the potential profiles of each of two barriers, photo-induced band bending effects in the contacts, as well as charge accumulation in the quantum well. In order to investigate the photoresponse of the single quantum well infrared photodetectors, we have fabricated GaAs/$Al_{0.3}Ga_{0.7}As$ single quantum well structures grown by molecular beam epitaxy. Steady state photoresponses of single quantum well infrared photodetectors have been discussed by a Fourier transform infrared spectroscopy. Furthermore, band bending effect due to a charge accumulation is shown by analysis of a dynamics of photo-induced carriers in single quantum well infrared photodetectors using a free electron laser beam, which has a wide tunability of the lasing wavelength and a short optical pulse. Numerical consideration of the SQWIP strongly supported the band bending effect due to photo-induced carriers.

Publication Lists

<International Journals>

1) K. Hirakawa, Y. Shimada, and T. Ikoma, "Supply-function dependent sequential resonant tunneling in semiconductor multiple quantum well diodes", Physica B **227** (1996) 202-205.

2) Y. Shimada and K. Hirakawa, "Sequential Resonant Magnetotunneling through Landau Levels in GaAs/AlGaAs Multiple Quantum Well Structures", Physica Status Solidi (B) **204** (1997) 427-430.

3) Y. Shimada and K. Hirakawa, "High-Field Domain Formation Condition in Semiconductor Multiple Quantum Well Sequential Resonant Tunneling Structures", Jpn. J. Appl. Phys. **36** (1997) 1012-1014.

4) Y. Shimada and K. Hirakawa, "Time Constant for High-Field Domain Formation in Multiple Quantum Well Sequential Resonant Tunneling Diodes", Jpn. J. Appl. Phys **36** (1997) 1944-1947.

5) Y. Shimada and K. Hirakawa, "Optical and Transport Properties of Single Quantum Well Infrared Photodetectors", Jpn. J. Appl. Phys. **37** (1998) 1421-1423.

6) Y. Shimada and K. Hirakawa, "Photocurrent Dynamics in Single Quantum Well Infrared Photodetectors Investigated by using Free Electron Laser Pulses", Nucl. Inst. Meth. Physics Research B **144** (1998) 166-171.

7) Y. Shimada, T. Matsuno, and K. Hirakawa, "Terahertz Emission due to Miniband Transport in GaAs/AlGaAs Superlattices", Jpn. J. Appl. Phys. **40** (2001) 3009-3011.

8) Y. Shimada and K. Hirakawa, "Time-resolved THz spectroscopy of miniband transport in biased GaAs/AlGaAs superlattices", Inst. Phys. Conf. Ser. **170** (2001) 395-400.

9) Y. Shimada, K. Hirakawa, and S.-W. Lee, "Time-resolved terahertz emission spectroscopy of wide miniband GaAs/AlGaAs superlattices", Appl. Phys. Lett. **81** (2002) 1642-1644.

10) Y. Shimada, K. Hirakawa, M. Odnoblioudov, and K. A. Chao, "Terahertz conductivity and possible Bloch gain in semiconductor superlattices", Phys. Rev. Lett. **90** (2003) 046806-1 - 4.

11) Y. Shimada, N. Sekine, and K. Hirakawa, "Inter-miniband resonant Zener tunneling in wide-miniband GaAs/$Al_{0.3}Ga_{0.7}As$ superlattices investigated by THz emission spectroscopy", Physica E **21** (2004) 661-665.

12) Y. Shimada, N. Sekine, and K. Hirakawa, "Terahertz emission due to inter-miniband resonant Zener tunneling in wide-miniband GaAs/$Al_{0.3}Ga_{0.7}As$ superlattices", Appl. Phys. Lett. **84** (2004) 4926-4928.

＜Domestic Journals＞

1) 島田洋蔵、平川一彦、「GaAs/AlGaAs多重量子井戸構造中のシークェンシャル・トンネリング」、電気学会研究会資料EFM-94, (1994) 57-65.

2) 島田洋蔵、「超格子について」、東大生研技術報告集Vol.7, (1998) 65-75.

3) 島田洋蔵、松野哲也、平川一彦、「相関測定法を用いたGaAs空乏層からの広帯域テラヘルツ光検出」、信学技報LQE-2000-4, (2000) 19-24.

＜International Journals (Others)＞

1) K. Tamura, K. Hirakawa, and Y. Shimada, "Drude absorption and electron localization in GaAs/AlGaAs superlattices", Physica B **272** (1999) 183-186.

2) S.-W. Lee, K. Hirakawa, and Y. Shimada, "Bound-to-continuum intersubband photoconductivity of self-assembled InAs quantum dots in modulation-doped heterostructures", Appl. Phys. Lett. **75**, (1999) 1428-1430.

3) S.-W. Lee, K. Hirakawa, and Y. Shimada, "Modulation-doped quantum dot infrared photodetectors using self-assembled InAs quantum dots ", Physica E **7**, (2000) 499-502.

4) S. Madhavi, M. Abe, Y. Shimada, and K. Hirakawa, "Nonequilibrium electron transport in wide miniband GaAs/AlGaAs superlattices at room temperature", Phys. Rev. B **65**, (2002) 193308-1 - 4.

5) M. Abe, S. Madhavi, Y. Shimada, Y. Otsuka, K. Hirakawa, and K. Tomizawa, "Transient carrier velocities in bulk GaAs : Quantitative comparison between terahertz data and ensemble Monte Carlo calculation", App. Phys. Lett. **81**, (2002) 679-681.

6) N. Sekine, Y. Shimada, and K. Hirakawa, "Dephasing mechanism of Bloch oscillations in GaAs/Al0.3Ga0.7As superlattices investigated by time-resolved terahertz spectroscopy", Appl. Phys. Lett. **83**, (2003) 4794-4796.

7) N. Sekine, Y. Shimada, K. Hirakawa, M. Odnoblioudov, and K. A. Chao, "Bloch gain in AlGaAs/GaAs semiconductor superlattices", Physica E **21** (2004) 858-862.

8) K. Jin, M. Odnoblyudov, Y. Shimada, K. Hirakawa, and K. A. Chao, "Terahertz frequency radiation from Bloch oscillations in GaAs/$Al_{0.3}Ga_{0.7}As$ superlattices", Phys. Rev. B **68**, (2003) 153315-1 – 4

＜Domestic Journal (Others)＞

1) 関根徳彦、島田洋蔵、平川一彦、「半導体超格子中のブロッホゲイン」、固体物理　39-2、(2004) 87-98.

＜International Conferences＞

1) Y. Shimada and K. Hirakawa, "Sequential Resonant Tunneling through Landau Levels in Modulation-Doped GaAs/$Al_{0.3}Ga_{0.7}As$ Multiple Quantum Wells", International Workshop on Mesoscopic Physics and Electronics (MPE '95), Tokyo, Japan, (March 6-8, 1995).

2) K. Hirakawa, Y. Shimada, and T. Ikoma, "Supply-function dependent sequential resonant tunneling in semiconductor multiple quantum well diodes", The Third International Symposium on "New Phenomena in Mesoscopic Structures", Hawaii, U.S.A., (December 4-8, 1995).

3) Y. Shimada and K. Hirakawa, "Time Constant for High-Field Domain Formation in Multiple Quantum Well Sequential Resonant Tunneling Diodes", 1996 International Conference on Solid State Devices and Materials (SSDM '96), Yokohama, Japan, (August 26-29, 1996).

4) Y. Shimada and K. Hirakawa, "Sequential Resonant Magnetotunneling through Landau Levels in GaAs/AlGaAs Multiple Quantum Well Diodes", 1997 International Conference on Nonequilibrium Carrier Dynamics in Semiconductors (HCIS-10), Berlin, Germany, (July 28-August 1, 1997).

5) Y. Shimada and K. Hirakawa, "Transport and Optical Properties of Single Quantum Well Infrared Photodetectors", 1997 International Conference on Solid State Devices and Materials (SSDM '97), Hamamatsu, Japan, (September 16-19, 1997).

6) Y. Shimada and K. Hirakawa, "Photocurrent Dynamics in Single Quantum Well Infrared Photodetectors Investigated by using Free Electron Laser Pulses", International Symposium on Free Electron Laser Facilities and Applications (FALFE '98), Kyoto, Japan, (January 26-29, 1998).

7) Y. Shimada, T. Matsuno, and K. Hirakawa "Broadband detection of THz radiation from semiconductor surfaces generated by femtosecond laser pulses", The 6^{th} International Workshop on Femtosecond Technology (FST '99), Makuhari, Japan, (July 13-15, 1999).

8) Y. Shimada, T. Matsuno, and K. Hirakawa, "Terahertz Emission due to Miniband Transport in GaAs/AlGaAs Superlattices", 2000 International Conference on Solid State Devices and Materials (SSDM 2000), Sendai, Japan, (August 29-31, 2000).

9) Y. Shimada, S. Madhavi, and K. Hirakawa, "THz emission from Bloch oscillations in wide miniband superlattices", International Symposium on Carrier Interactions in Mesoscopic Systems (CIM 2001), Atsugi, Japan, (February 13-14, 2001).

10) Y. Shimada and K. Hirakawa, "Time-resolved THz spectroscopy of miniband transport in biased GaAs/AlGaAs superlattices", The 28th International Symposium on Compound Semiconductors (ISCS 2001), Tokyo, Japan, (Octobert 1-4, 2001).

11) K. Hirakawa and Y. Shimada, "Dynamical carrier transport in semiconductor superlattices –Gain in the Terahertz regime-", The second International Workshop on Quantum Nonplaner Nanostructures & Nanoelectronics '02 (QNN '02), Tsukuba, Japan, (September 9-11, 2002).

12) Y. Shimada and K. Hirakawa, "Crossover of miniband, Wannier-Stark quantization, and Zener tunneling regimes in wide miniband superlattices investigated by time-resolved terahertz spectroscopy", The 26th International Conference on the Physics of Semiconductors (ICPS 2002), Edinburgh, UK, (July 30-August 2, 2002).

13) Y. Shimada and K. Hirakawa, "Miniband, Wannier-Stark Quantization, and Zener Breakdown in Wide Miniband Superlattices Investigated by Time-Domain Terahertz Spectroscopy", International Conference on Solid State Devices and Materials (SSDM 2002), Nagoya, Japan, (September 17-20, 2002).

14) Y. Shimada, N. Sekine, and K. Hirakawa, "Inter-Miniband Resonant Zener Tunneling in Wide-Miniband GaAs/AlGaAs Superlattices Investigated by THz Emission Spectroscopy", The 11th International Conference on Modulated Semiconductor Structure (MSS11), Nara, Japan (July 14-18, 2003).

15) Y. Shimada, N. Sekine, and K. Hirakawa, "THz Emission Spectroscopy of Inter-Miniband Resonant Zener Tunneling in Wide-Miniband GaAs/$Al_{0.3}Ga_{0.7}As$ Superlattices", 11th International Conference on Terahertz Electronics (THz2003), Sendai, Japan (September 24-26, 2003).

<International Conferences (Others)>

1) S.-W. Lee, K. Hirakawa, and Y. Shimada, "Intersubband Transition Spectroscopy of Self-Assembled InAs Quantum Dots", The 2nd International Symposium on Formation, Physics and Device Application of Quantum Dot Structure (QDS '98), Sapporo, Japan, (1998).

2) T. Matsuno, Y. Shimada, and K. Hirakawa, "Intense broadband terahertz radiation from biased GaAs p-i-n structures generated by femtosecond laser pulses", The 7th IEEE International Conference on Terahertz Electronics (THz 99), Nara, Japan, (1999)

3) K. Tamura, K. Hirakawa, and Y. Shimada, "Drude absorption and electron localization in GaAs/AlGaAs superlattices", The 11th International Conference of Nonequilibrium Carrier Dynamics in Semiconductors, Kyoto, Japan, (July 19-23, 1999).

4) S.-W. Lee, K. Hirakawa, and Y. Shimada, "Modulation-Doped Quantum Dot Infrared Photodetectors Using Self-Assembled InAs Quantum Dots", The 9th International Conference on Modulated Semiconductor Structure (MSS9), Fukuoka, Japan, (1999).

5) S.-W. Lee, K. Hirakawa, and Y. Shimada, "Bound-to-Continuum Intersubband Transition in Self-Assembled InAs Quantum Dots and Its Application to Mid-Infrared Photodetectors", The 5th International Conference on Intersubband Transition in Quantum Wells (ITQW '99), Bad Ischl, Austria, (1999).

6) S.-W. Lee, K. Hirakawa, Ph. Lelong, Y. Shimada, and H. Sakaki "Mid-Infrared Photodetection of Fano Resonance in Bound-to-Continuum Intersubband Transition in Self-Assembled InAs Quantum Dots", International conference on Solid State Devices and Materials (SSDM '99), Tokyo, Japan, (1999).

7) S.-W. Lee, K. Hirakawa, and Y. Shimada, "Mid-Infrared Photodetector Using Self-Assembled InAs Quantum Dots Embedded In Modulation Doped GaAs Quantum Wells", (MRS '99), Boston, USA, (1999).

8) K. Hirakawa, N. Sekine, Y. Shimada, M. Vosseburger, P. Haring-Bolivar, and H. Kurz, "Impulsive Excitation of Two-dimensional Plasmons by Femtosecond Laser Pulses", CREST Workshop on "Physics and Application of Quantum Dots", Hakone, Japan, (October 14-16, 1999).

9) S.-W. Lee, K.Hirakawa, and Y. Shimada, "Mid-Infrared Photodetector using Self-Assembled InAs Quantum Dots Embedded in Modulation-doped GaAs Quantum Wells", Materials Research Society Symposium Proceedings Vol. 607 Infrared Applications of Semiconductors III, pp147-152 (2000).

10) M. Abe, S. Madhavi, Y. Shimada, K. Hirakawa, and K. Tomizawa, "Transient velocity of electrons in GaAs investigated by time-domain THz spectroscopy", 12th International Conference on Nonequilibrium Carrier Dynamics in Semiconductors (HCIS-12), Santa Fe, U.S.A., (August 27-31, 2001).

11) S. Madhavi, M. Abe, Y. Shimada, and K. Hirakawa, "Room temperature miniband transport in GaAs/AlGaAs superlattice structures", 12th International Conference on Nonequilibrium Carrier Dynamics in Semiconductors (HCIS-12), Santa Fe, U.S.A., (August 27-31, 2001).

12) N. Sekine, Y. Shimada, K. Hirakawa, M. Odnoblioudov, and A. Chao, "Bloch Gain in AlGaAs/GaAs Semiconductor Superlattices", The 11th International Conference on Modulated Semiconductor Structure (MSS11), Nara, Japan, (July 14-18, 2003).

13) N. Sekine, Y. Shimada, K. Hirakawa, M. Odnoblioudov, and A. Chao, "Bloch gain in AlGaAs/GaAs semiconductor superlattices investigated by time-domain THz emission spectroscopy", 11th International Conference on Terahertz Electronics (THz2003), Sendai, Japan, (September 24-26, 2003).

14) N. Sekine, Y. Shimada, and K. Hirakawa, "Relaxation Mechanisms of Bloch oscillations in AlGaAs/GaAs Superlattices Investigated by Time-Domain Terahertz Spectroscopy", The 7th International Conference on Intersubband Transitions in Quantum Wells (ITQW2003), Switzerland, (September 1-5, 2003).

15) K. Hirakawa, N. Sekine, Y. Shimada, M. Odnoblioudov, and A. Chao, "Bloch Gain in Semiconductor Superlattices", The 28th International Conference on Infrared and Millimeter Waves (IMW2003), Otsu, Japan, (September 29 – October 1, 2003).

＜Domestic Conferences＞

1) 島田洋蔵、平川一彦、「GaAs／AlGaAs 多重量子井戸構造中のシークェンシャル・トンネリング」、電気学会研究会資料（電子材料研究会） EFM-94-7~15、 Tokyo、 (September, 1994) 57.

2) 島田洋蔵、平川一彦、生駒俊明、「GaAs／AlGaAs 超格子構造中の高電界ドメイン」、第５４回応用物理学会学術講演会 29p-ZX-12、北海道大学、 (September, 1993).

3) 島田洋蔵、平川一彦、生駒俊明、「GaAs／AlGaAs 多重量子井戸構造中の高電界ドメイン(II)」、第４１回応用物理学関係連合講演会 30a-S-7、 明治大学、(March, 1994).

4) 島田洋蔵、平川一彦、「GaAs／AlGaAs 多重量子井戸構造中の高電界ドメイン(III)」、第５５回応用物理学会学術講演会 21a-T-8、名城大学、(September, 1994).

5) 島田洋蔵、平川一彦、「GaAs／AlGaAs 多重量子井戸構造中の高電界ドメイン形成のダイナミクス」、第５６回応用物理学会学術講演会 29p-ZM-3、金沢大学、(September, 1995).

6) 島田洋蔵、平川一彦、「強磁場中における半導体多重量子井戸構造中の供給関数とシークェンシャル共鳴トンネル現象」、重点領域研究「量子位相エレクトロニクス」第５回研究会、箱根、(September, 1995).

7) 島田洋蔵、平川一彦、「半導体多重量子井戸トンネル構造中の高電界ドメイン形成の供給関数依存性」、第４３回応用物理学関係連合講演会 29p-W-16、東洋大学、(March, 1996).

8) 島田洋蔵、平川一彦、「半導体多重量子井戸トンネル構造中の高電界ドメイン形成のダイナミクス」、第５７回応用物理学会学術講演会 9p-ZC-6、九州産業大学、 (September, 1996).

9) 島田洋蔵、平川一彦、山中宏治、関根徳彦、「単一量子井戸赤外フォトディテクターの光応答」、第４４回応用物理学関係連合講演会 28a-ZA-3、日本大学船橋校舎、(March, 1997).

10) 島田洋蔵、平川一彦、「自由電子レーザー照射による単一量子井戸赤外フォトディテクターの評価」、第５８回応用物理学会学術講演会 4p-ZF-4、秋田大学、(October, 1997).

11) 島田洋蔵、平川一彦、「単一量子井戸赤外フォトディテクターの動作解析」、第５９回応用物理学会学術講演会 16a-ZN-8、広島大学、(September, 1998).

12) 島田洋蔵、「超格子について」、東大生研第７回技術発表会、六本木、(September 22, 1998).

13) 島田洋蔵、松野哲也、平川一彦、「フェムト秒レーザー照射によるInAsからのTHz発光の広帯域検出」、第６０回応用物理学会学術講演会 4a-G-4、甲南大学、(September, 1999).

14) 島田洋蔵、松野哲也、関根徳彦、平川一彦、「フェムト秒レーザー照射による半導体表面からの超短パルステラヘルツ発光」、第３回テラフォトニクス研究会、松島、(September 16-17, 1999).

15) 島田洋蔵、松野哲也、平川一彦、荒川泰彦、「GaAs/AlGaAs半導体超格子構造中のミニバンド伝導とテラヘルツ放射」、第４７回応用物理学関係連合講演会、青山学院大学、(March, 2000).

16) 島田洋蔵、松野哲也、平川一彦、「相関測定法を用いたGaAs空乏層からの広帯域テラヘルツ光検出」、電子情報通信学会技術研究報告（レーザー・量子エレクトロニクス研究会） LQE 2000-4, (2000).

17) Y. Shimada, S. Madhavi, T. Matsuno, M. Abe, and K. Hirakawa, "Ultrafast transient electron transport in semiconductor depletion layers and superlattices investigated by time-domain THz spectroscopy", The First CREST Symposium on "Functional Evolution of Materials and Devices based on Electron/Photon Related Phenomena", Tokyo, (October 2000).

18) 島田洋蔵、平川一彦、「広ミニバンドGaAs/AlGaAs超格子中のブロッホ振動によるテラヘルツ放射」、第４８回応用物理学関係連合講演会 28p-YD-10、明治大学、(March, 2001).

19) Y. Shimada, S. Madhavi, M. Abe, and K. Hirakawa, "Time-domain THz spectroscopy of miniband transport in GaAs/AlGaAs superlattices", The Second CREST Symposium on "Functional Evolution of Materials and Devices based on Electron/Photon Related Phenomena", Tokyo, (October 2001).

20) 島田洋蔵、平川一彦、「時間分解テラヘルツ分光法によるGaAs/AlGaAs超格子中のブロッホ振動の評価」、春季第４９回応用物理学関係連合講演会 27a-YH-11、東海大学、(March, 2002).

21) 平川一彦、島田洋蔵、「GaAs/AlGaAs超格子中のブロッホ振動電子と電磁波に対するゲイン」、第６３回応用物理学会学術講演会 29a-ZE-8、新潟大学、(September, 2002).

22) 島田洋蔵、関根徳彦、平川一彦、「GaAs/AlGaAs超格子中のミニバンド間共鳴ツェナートンネリング」、第５０回応用物理学関係連合講演会 29a-ZE-8、神奈川大学横浜キャンパス、(March, 2003).

＜Domestic Conferences (Others)＞

1) 平川一彦、李　承雄、島田洋蔵、「自己組織化InAs量子ドットの赤外サブバンド間遷移スペクトロスコピー」、重点領域研究「単電子デバイスとその高密度集積化」平成９年度第３回研究会、名古屋大学、(January 26-27, 1998).

2) 李　承雄、平川一彦、島田洋蔵、「自己組織化InAs量子ドットの赤外サブバンド間遷移スペクトロスコピー」、第４５回応用物理学会関係連合講演会、30a-PC-2、東京工科大学、(March, 1998).

3) 田村航一、平川一彦、島田洋蔵、「GaAs/AlGaAs超格子の縦方向ドルーデ遠赤外光吸収」、第５９回応用物理学会学術講演会、広島大学、(September, 1998).

4) 関根徳彦、平川一彦、島田洋蔵、「時間分解THz分光法による量子構造中の超高速現象の研究」、第２回「量子効果等に関する物理現象」、JAホール（東京）、(December 21-22, 1998).

5) 平川一彦、李　承雄、島田洋蔵、「自己組織化InAs量子ドットを用いた横方向伝導型赤外光検出器」、特定領域(A)「単電子デバイスとその高密度集積化」第３回研究会、筑波大学、(January 25-26, 1999).

6) 田村航一、平川一彦、島田洋蔵、「GaAs/AlGaAs超格子中のDrude伝導と電子の局在」、第４６回応用物理学関係連合講演会、東京理科大学、(March, 1999).

7) 李　承雄、平川一彦、島田洋蔵、「自己組織化InAs量子ドットを用いた変調ドープ横方向伝導型赤外光検出器」、第４６回応用物理学会関係連合講演会、29p-ZL-9、東京理科大学、(March, 1999).

8) 李　承雄、平川一彦、島田洋蔵、「自己組織化InAs量子ドットを用いた変調ドープ横方向伝導型赤外光検出器」、電子情報通信学会技術研究報告（レーザー・量子エレクトロニクス研究会）、LQE-99、機会振興会館、(June 23, 1999)　29-34.

9) 松野哲也、島田洋蔵、平川一彦「フェムト秒レーザー励起によるPIN構造からのTHz電磁波の発生」、第６０回応用物理学会学術講演会、甲南大学、(September, 1999).

10) 李　承雄、平川一彦、島田洋蔵、「自己組織化InAs量子ドットを用いたBound-to-Continuumサブバンド間遷移赤外光検出」、第６０回応用物理学会学術講演会、4p-ZL-9、甲南大学、(September, 1999).

11) 平川一彦、李　承雄、Ph. Lelong、島田洋蔵、榊　裕之、「自己組織化InAs量子ドット中のサブバンド間遷移とFano共鳴」、特定領域研究(A)「単電子デバイスとその高密度集積化」平成１１年度第２回研究会、六本木（東京）、(November 4-5, 1999).

12) 松野哲也、島田洋蔵、平川一彦、荒川泰彦、「低温成長GaAs MIN構造からのフェムト秒レーザ励起によるTHz電磁波の発生」第４７会応用物理学関係連合講演会、青山学院大学、(March, 2000).

13) 李　承雄、平川一彦、島田洋蔵、「横方向伝導型量子ドット赤外検出器：光キャリアの寿命と感度」、第４７回応用物理学会関係連合講演会、31p-K-4、青山学院大学 (March 2000).

14) 阿部真理、S.マダビ、島田洋蔵、平川一彦、「時間分解THｚ分光法を用いたGaAs中の速度オーバーシュートの評価」、第４８回応用物理学関係連合講演会 28p-YD-13、明治大学、(March, 2001).

15) S. Madhavi, M. Abe, Y. Shimada, and K. Hirakawa, "Electro-optic detection of miniband transport in GaAs/AlGaAs superlattices"、第４８回応用物理学関係連合講演会 29p-V-10、明治大学、(March, 2001).

16) 平川一彦、島田洋蔵、阿部真理、S.マダビ、「テラヘルツ電磁放射で探る半導体中の超高速キャリアダイナミクス」、第４９回応用物理学関係連合講演会 29p-YQ-6、東海大学 (March 2002).

17) 阿部真理、S.マダビ、島田洋蔵、平川一彦、富沢一隆、「時間分解THz分光法によるキャリア速度評価とモンテカルロ計算の比較」、第４９回応用物理学関係連合講演会 29a-P8-17、東海大学 (March 2002).

18) 阿部真理、S.マダビ、島田洋蔵、平川一彦、「時間分解THｚ分光法によるGaAsチャネル中のキャリア走行時間の評価」、第４９回応用物理学関係連合講演会 29a-YK-3、東海大学 (March 2002).

19) 長嶋知行、S. Madhavi、島田洋蔵、平川一彦、「半導体超格子中のブロッホ電子の過渡伝導解析」、第５０回応用物理学関係連合講演会 28p-ZE-1、神奈川大学横浜キャンパス (March 2003).

20) 関根徳彦、島田洋蔵、平川一彦、「半導体超格子中のブロッホ振動における緩和時間の温度依存性」、第５０回応用物理学関係連合講演会 28p-ZE-2、神奈川大学横浜キャンパス (March 2003).

21) 関根徳彦、島田洋蔵、平川一彦、「テラヘルツ電気光学サンプリング法による半導体超格子中のブロッホ振動の観測」、第６４回応用物理学会学術講演会、(August 2003).

22) 関根徳彦、島田洋蔵、平川一彦、「テラヘルツ電気光学サンプリング法による半導体超格子中のブロッホ振動の観測(II)」、第５１回応用物理学関係連合講演会 29p-ZE-6、東京工科大学 (March 2004).